

## RESEARCH LETTER

10.1002/2014GL062366

## Key Points:

- Detection of multivariable signals of recent volcanic activity in observations
- Volcanic signals are identifiable in both the late 20th and early 21st centuries
- Successful volcanic signal detection depends on removal of ENSO variability

## Supporting Information:

- Figures S1–S11 and Table S1

## Correspondence to:

B. D. Santer,  
santer1@llnl.gov

## Citation:

Santer, B. D., et al. (2015), Observed multivariable signals of late 20th and early 21st century volcanic activity, *Geophys. Res. Lett.*, 42, doi:10.1002/2014GL062366.

Received 29 OCT 2014

Accepted 24 DEC 2014

Accepted article online 29 DEC 2014

## Observed multivariable signals of late 20th and early 21st century volcanic activity

Benjamin D. Santer<sup>1</sup>, Susan Solomon<sup>2</sup>, Céline Bonfils<sup>1</sup>, Mark D. Zelinka<sup>1</sup>, Jeffrey F. Painter<sup>1</sup>, Francisco Beltran<sup>1</sup>, John C. Fyfe<sup>3</sup>, Gardar Johannesson<sup>1</sup>, Carl Mears<sup>4</sup>, David A. Ridley<sup>2</sup>, Jean-Paul Vernier<sup>5</sup>, and Frank J. Wentz<sup>4</sup>

<sup>1</sup>Program for Climate Model Diagnosis and Intercomparison, Lawrence Livermore National Laboratory, Livermore, California, USA, <sup>2</sup>Earth, Atmospheric, and Planetary Sciences, Massachusetts Institute of Technology, Cambridge, Massachusetts, USA, <sup>3</sup>Canadian Centre for Climate Modelling and Analysis, Environment Canada, Victoria, British Columbia, Canada, <sup>4</sup>Remote Sensing Systems, Santa Rosa, California, USA, <sup>5</sup>NASA Langley Research Center, Hampton, Virginia, USA

**Abstract** The relatively muted warming of the surface and lower troposphere since 1998 has attracted considerable attention. One contributory factor to this “warming hiatus” is an increase in volcanically induced cooling over the early 21st century. Here we identify the signals of late 20th and early 21st century volcanic activity in multiple observed climate variables. Volcanic signals are statistically discernible in spatial averages of tropical and near-global SST, tropospheric temperature, net clear-sky short-wave radiation, and atmospheric water vapor. Signals of late 20th and early 21st century volcanic eruptions are also detectable in near-global averages of rainfall. In tropical average rainfall, however, only a Pinatubo-caused drying signal is identifiable. Successful volcanic signal detection is critically dependent on removal of variability induced by the El Niño–Southern Oscillation.

## 1. Introduction

A number of scientific explanations have been advanced for the post-1998 “hiatus” in surface and tropospheric warming. One prominent view is that this behavior is primarily or wholly attributable to natural internal variability of the climate system, originating in either the eastern equatorial Pacific Ocean [Kosaka and Xie, 2013] or in both the Pacific and Atlantic Oceans [Chen and Tung, 2014]. Other interpretations of the “hiatus” posit that the relatively muted surface and tropospheric warming over the past 17 years is not due to a single cause but instead arises from the combined effects of internal variability and external forcing [Solomon et al., 2011; Fyfe et al., 2013a, 2013b; Flato et al., 2013; Santer et al., 2014; Schmidt et al., 2014; Huber and Knutti, 2014; Trenberth et al., 2014].

The external factors that have received most attention in “hiatus” studies are 21st century increases in volcanic aerosol forcing [Solomon et al., 2011; Vernier et al., 2011; Neely et al., 2013; Fyfe et al., 2013a; Santer et al., 2014; Ridley et al., 2014], the unusually long and low minimum in solar irradiance during the last solar cycle [Kopp and Lean, 2011], changes in stratospheric water vapor [Solomon et al., 2010], and an increase in emissions of anthropogenic sulfate aerosols [Kaufmann et al., 2011; Schmidt et al., 2014]. Several recent modeling studies which consider more realistic post-1998 changes in these external factors—in combination with internal variability—are capable of explaining most of the observed “hiatus” [Fyfe et al., 2013b; Schmidt et al., 2014]. Uncertainties remain, however, and another modeling study suggests that key seasonal features of the “hiatus” are primarily attributable to changes in the Pacific Decadal Oscillation [Trenberth et al., 2014]. Reliable quantitative partitioning of different external and internal contributions to the “hiatus” is still urgently required.

Here we extend earlier research on the contribution of early 21st century volcanic forcing to the “hiatus” [Solomon et al., 2011; Fyfe et al., 2013a]. Recently, Santer et al. [2014] detected signals of 21st century volcanic forcing in observations of the temperature of the lower troposphere (TLT) and net clear-sky short-wave radiation at the top of the atmosphere (SW). We consider whether volcanic signal detection is feasible for four additional observational variables: sea surface temperature (SST), the temperature of the middle to upper troposphere (TMT), column-integrated water vapor (PW), and precipitation (PR). While several previous studies identified a statistically significant signal of 20th century volcanic activity in observational

precipitation records [Gillett *et al.*, 2004; Iles and Hegerl, 2014], our analysis is the first to search for signals of 21st century volcanic forcing in observational PW and PR data.

## 2. Observational Data

We use stratospheric aerosol optical depth (SAOD) data from Vernier *et al.* [2011] to study changes in stratospheric loadings of volcanic aerosol. The Vernier *et al.* [2011] SAOD data are from three different sets of satellite-based aerosol measurements: (1) Stratospheric Aerosol and Gas Experiment, phase II (SAGE II; January 1985 to August 2005); (2) Global Ozone Monitoring by Occultation of Stars (GOMOS; September 2005 to May 2006); and (3) Cloud-Aerosol Lidar and Infrared Pathfinder Satellite Observations (CALIPSO; June 2006 to December 2013). Monthly mean SAOD data are in the form of zonal averages for 5° latitude bands, with coverage extending from 50°N to 50°S. Data were available for the 348 month period from January 1985 to December 2013. The altitude range of the measurements is 15 to 40 km. Volcanic signals from portions of the stratosphere below 15 km are not included in this analysis [Ridley *et al.*, 2014].

We consider the influence of SAOD on the six climate variables mentioned above. We use SST data from version 3b of the National Oceanic and Atmospheric Administration (NOAA) Extended Reconstructed Sea Surface Temperature data set [Smith *et al.*, 2008]. TMT and TLT data sets are based on satellite measurements made by Microwave Sounding Units on NOAA polar-orbiting satellites; data were made available by Remote Sensing Systems (RSS) [Mears *et al.*, 2011]. RSS also provided estimates of column-integrated water vapor over oceans, which rely on measurements made by the satellite-borne Special Sensor Microwave Imager (SSM/I) [Mears *et al.*, 2007]. Precipitation information is from version 2.2 of the data set produced by the Global Precipitation Climatology Project; the data set is based on both in situ and satellite measurements [Adler *et al.*, 2003].

Finally, we used Edition 2.8 of the Energy Balance and Filled (EBAF) Clouds and Earth's Radiant Energy System (CERES) net clear-sky SW radiation data [Loeb *et al.*, 2009]. We show clear-sky results to avoid obfuscating cloud effects. Our use of net SW radiation accounts for variations in both the upwelling and downwelling components of SW. Upwelling arises due to backscatter from the surface and the atmosphere, while downwelling is associated with changes in solar irradiance over the 11 year solar cycle. In the supporting information (SI), we also analyze net clear-sky SW fluxes from the International Satellite Cloud Climatology Project (ISCCP) FD data set [Zhang *et al.*, 2004].

We seek to determine whether volcanic signals are identifiable in large-scale spatial averages of observed climate records. We examine averages over the tropics (20°N–20°S), where most of the larger early 21st century volcanic eruptions occurred [Vernier *et al.*, 2011; Neely *et al.*, 2013], and over the 50°N–50°S domain covered by the Vernier *et al.* SAOD data.

Because of the high emissivity of the land surface, SSM/I PW data are available over ocean only. To facilitate the comparison of PW and SST with other climate variables, observational TMT, TLT, and PR data were masked out over land before calculating tropical and near-global spatial averages. Masking of land areas is not required for upper atmosphere quantities (SAOD and SW).

## 3. Statistical Removal of El Niño–Southern Oscillation Effects

Large volcanic eruptions increase the loadings of liquid-phase sulfate aerosol particles in the stratosphere, leading to backscattering of incoming solar radiation [Robock, 2000; Ramaswamy *et al.*, 2006] and to a decrease in net absorbed clear-sky SW radiation at the top of the atmosphere [Soden *et al.*, 2002; Harries and Futyran, 2006]. The resulting cooling of the surface and troposphere yields drying signals in atmospheric water vapor [Soden *et al.*, 2002] and in rainfall [Broccoli *et al.*, 2003; Gillett *et al.*, 2004; Iles and Hegerl, 2014]. These cooling and drying signals are partly obscured by internally generated variability of the climate system. In the tropics, the largest contribution to the interannual variability of temperature and moisture is from the El Niño–Southern Oscillation (ENSO). Statistical removal of ENSO effects more clearly reveals the underlying climate signals caused by volcanic activity [Wigley, 2000; Santer *et al.*, 2001; Soden *et al.*, 2002; Wigley *et al.*, 2005; Thompson *et al.*, 2009; Santer *et al.*, 2014].

We apply the iterative regression-based method of Wigley [2000] and Santer *et al.* [2001] to remove ENSO effects from the spatially averaged TMT, TLT, SST, PW, and PR data. The method accounts for collinearity between the predictor variables used to estimate ENSO and volcano signals, as well as for modulation of

the volcanically forced surface and tropospheric temperature changes by the thermal inertia of the ocean. Because ENSO has no discernible influence on tropical SAOD, and explains only a small fraction (less than 5%) of the temporal variance of net clear-sky SW fluxes at the top of the atmosphere, we do not remove ENSO effects from either the SAOD or SW time series.

#### 4. SAOD and Climate Time Series

In both the tropical (Figure 1a) and near-global averages (Figure 1h), there is a gradual increase in SAOD over the first 13 years of the 21st century, driven by the cumulative effects of a succession of “moderate” volcanic eruptions [Vernier *et al.*, 2011; Solomon *et al.*, 2011]. Superimposed on this gradual secular change are SAOD increases associated with some of the larger recent eruptions: Manam (January 2005), Soufrière Hills and Tavurvur (May/October 2006), Sarychev (June 2009), Merapi (October 2010), and Nabro (June 2011). The signatures of Tavurvur and Nabro are visually obvious in the CERES SW data (Figures 1b and 1i), as well as in temperature and moisture data averaged over the tropics (Figures 1c–1g) and the near-global domain (Figures 1j–1n).

Even after statistical removal of ENSO effects, however, there is still considerable residual monthly to interannual-timescale variability. This variability has multiple sources, including the following: (1) internal variability from sources other than ENSO; (2) incomplete removal of ENSO effects [Santer *et al.*, 2001]; (3) changes over time in atmospheric loadings of anthropogenic aerosols; and (4) volcanic forcing. It is visually obvious from Figures 1 and S1 that the residual variability of temperature and moisture is larger in tropical averages than in near-global means. This difference in noise levels is particularly apparent for precipitation, and partly explains why the PR signals arising from “moderate” 21st century eruptions are more easily identifiable in near-global averages (see below).

#### 5. Assessing Statistical Significance

We use the approach of Santer *et al.* [2014] to investigate the behavior and statistical significance of  $r\{S, X\}$ , the correlation between  $S(t)$  (the observed time series of SAOD) and  $X(t)$  (the climate variable of interest).

Here  $X(t)$  is one of the six temperature, moisture, or radiation variables in Figure 1. Because volcanic activity is nonstationary, the strength of the linear relationship between SAOD and  $X(t)$  is sensitive to the specific analysis period (see Figure 1a). We address the nonstationarity of SAOD by sliding maximally overlapping 60 month windows through the  $S(t)$  and  $X(t)$  time series. We calculate  $r_i\{S, X\}$  for each window, after first removing ENSO effects from all temperature and moisture variables. The index  $i$  runs over  $n_i$ , the total number of windows (see SI).

While SW responds very rapidly to changes in SAOD, the responses of SST and tropospheric temperature and moisture typically lag the volcanic forcing [Santer *et al.*, 2001; Wigley *et al.*, 2005]. We therefore calculate  $r_i\{S, X\}$  for contemporaneous time series of SAOD and SW, but for all other climate variables, we stipulate that  $X$  lags SAOD and examine  $r_i\{S, X\}$  results for lags ranging from 1 to 3 months.

To determine whether large negative correlations could be due to chance alone, we rely on null distributions of  $r_i\{S, X^*\}$  obtained with synthetic  $X(t)^*$  data, as in Santer *et al.* [2014]. Here and subsequently, an asterisk denotes a statistic calculated with synthetic  $S(t)^*$  or  $X(t)^*$  time series. For each climate variable, 10,000 realizations of synthetic  $X(t)^*$  data were generated with a standard lag-1 autoregressive (AR-1) model:

$$X(t)^* = a_1 X(t-1)^* + Z(t) ; t = 1, \dots, n_t \quad (1)$$

where  $a_1$  is the coefficient of the AR-1 model,  $Z(t)$  represents randomly generated white noise, and  $n_t$  is the length of the climate time series. We removed ENSO effects from each climate variable except SW and then estimated  $a_1$  from  $X_q(t)$ , a volcanically quiescent portion of the observations (see SI).

Synthetic climate data were processed in an analogous way to the observations. For each realization of  $X(t)^*$ , we calculated  $r_i\{S, X^*\}$  using maximally overlapping 60 month segments of the observed SAOD data and the contemporaneous or lagged synthetic climate data. This yielded separate 10,000-member null distributions of  $r_i\{S, X^*\}$  for each climate variable, each 60 month pair of SAOD and  $X(t)^*$  segments, each time lag considered, and each averaging domain. Empirical  $p$  values were determined by comparing the

## Changes in Optical Depth, Radiation, Temperature, and Moisture

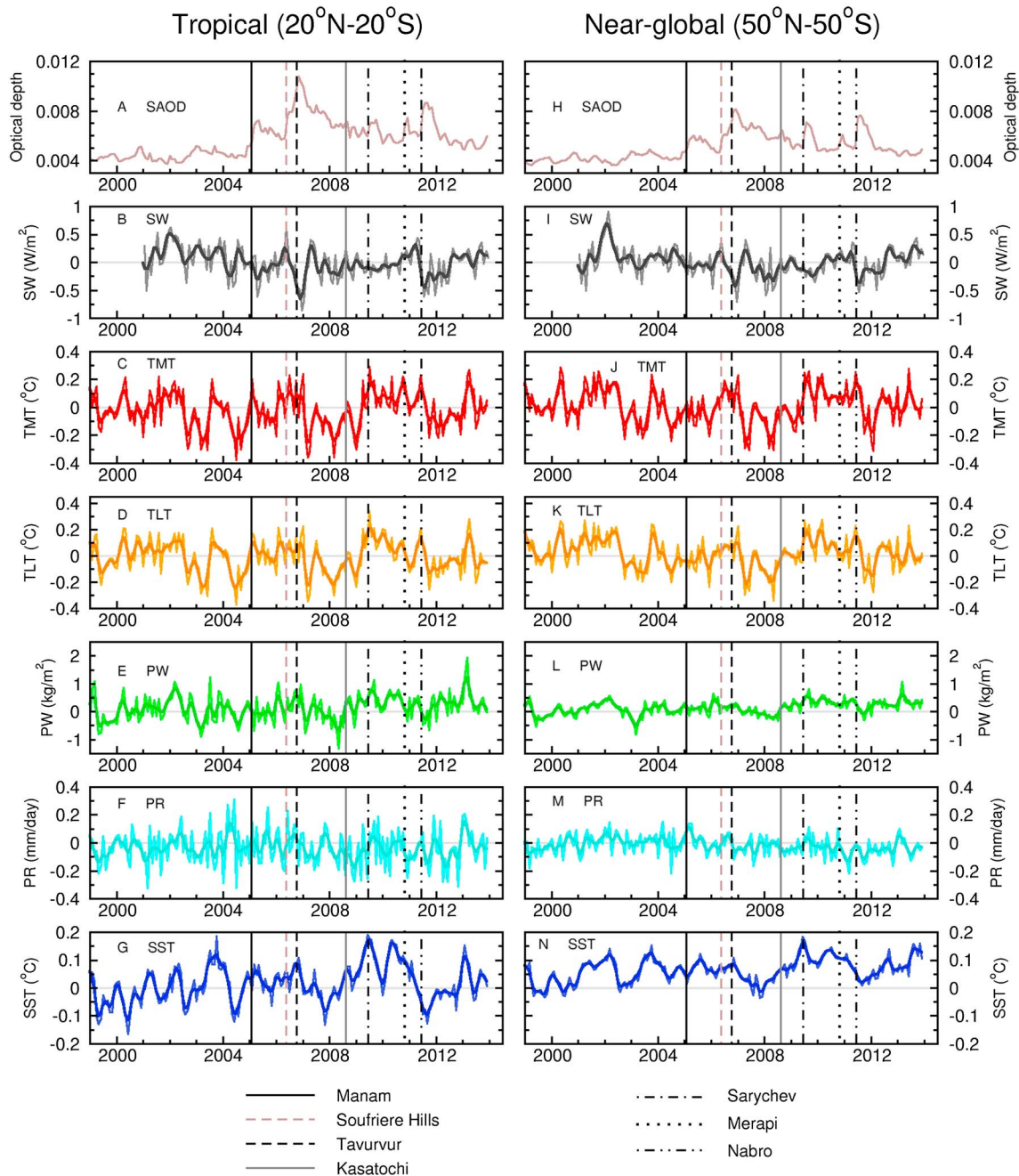


**Figure 1.** Time series of early 21st century changes in observations of (a, h) stratospheric aerosol optical depth (SAOD) and (b, i) net clear-sky short-wave radiation at the top of the atmosphere (SW) and “ENSO removed” (c, j) middle to upper tropospheric temperature (TMT), (d, k) lower tropospheric temperature (TLT), (e, l) column-integrated water vapor (PW), (f, m) rainfall rate (PR), and (g, n) sea surface temperature (SST). Results in the left (right) column are spatially averaged over tropical (near-global) oceans except in the case of SAOD and SW data, which are averaged over both land and ocean. The tropical and near-global domains are 20°N–20°S and 50°N–50°S, respectively. Anomalies of TMT, TLT, PW, PR, and SST are defined relative to climatological monthly means for the longest period of common coverage (January 1988 to December 2013). SW results were only available for a shorter period and are expressed as anomalies relative to climatological monthly averages over January 2001 to December 2013. SAOD data are not in anomaly form. In the sign convention used here and elsewhere [Soden *et al.*, 2002; Harries and Futyran, 2006], negative SW anomalies denote a decrease in the net absorbed solar radiation. A five-term binomial filter was used to produce the smoothed results (bold lines). Vertical lines denote the dates of seven selected early 21st century eruptions. The peak SAOD in November/December 2006 is due to the combined effect of Soufrière Hills (May 2006) and Tauruvur (October 2006).

Correlation: SAOD and Temperature/Moisture/Radiation

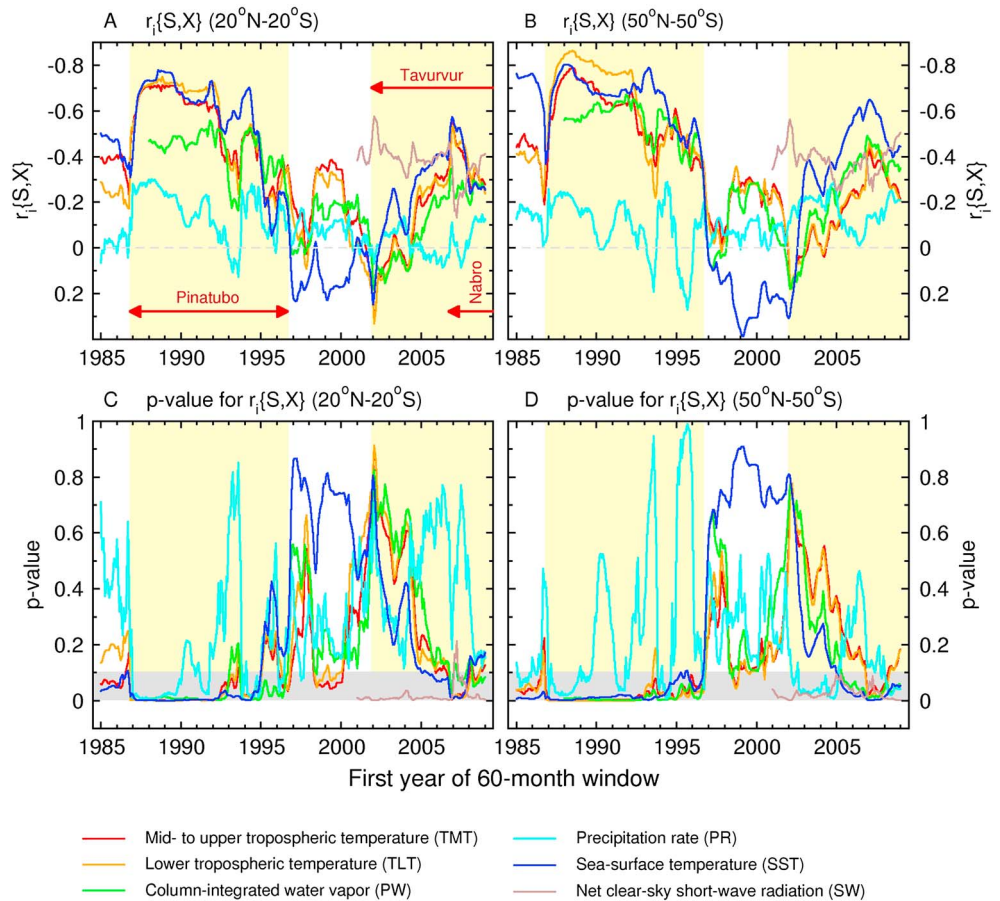


**Figure 2.** Behavior of the (a, b) correlation statistic  $r_i\{S, X\}$  and (c, d) associated  $p$  values. Correlations between SAOD and climate variable  $X$  were calculated using data spatially averaged over the tropics (left column) and over a near-global domain (right column). Values of  $r_i\{S, X\}$  were computed using a 60 month moving window, with overlap of 59 months between successive analysis periods; the index  $i$  runs over the number of windows. For all variables except SAOD and SW, ENSO effects were statistically removed prior to calculating  $r_i\{S, X\}$ . Correlations between SAOD and SW are contemporaneous; in all other cases, temperature and moisture time series lag SAOD by 2 months. The statistical significance of  $r_i\{S, X\}$  was assessed as described in the SI. Values of  $r_i\{S, X\}$  within the grey shaded box in Figures 2c and 2d are significant at the 10% level or better and are unlikely to occur by chance alone. Each panel has two yellow boxes, which are centered on  $SAOD_{PIN}(t)$  and  $SAOD_{TAV}(t)$ , the months of the maximum SAOD after the eruptions of Pinatubo (left yellow box) and Soufrière Hills/Tavurvur (right yellow box). The bounds of each yellow box are the month of maximum SAOD  $\pm 59$  months; i.e., the box width spans the range of start dates for all 60 month moving windows which sample either  $SAOD_{PIN}(t)$  or  $SAOD_{TAV}(t)$ . The beginning of the period influenced by the June 2011 eruption of Nabro is indicated in Figure 2a. Slight vertical displacement of the x axis in Figures 2c and 2d allows easier visual identification of  $p$  values close to zero.

observed  $r_i\{S, X\}$  results with their respective null distributions. Full details of the significance testing procedure are provided in the SI.

**6. Results From Significance Tests**

We first consider  $r_i\{S, X\}$  results for the tropics and the near-global domain (Figures 2a and 2b, respectively). Values of  $r_i\{S, X\}$  are predominantly negative, with pronounced temporal variability. This variability is correlated across different climate variables. The largest negative correlations occur during 60 month periods which sample the effects of the June 1991 Pinatubo eruption. These anticorrelations reflect concurrent increases in SAOD and decreases in tropospheric temperature, SST, atmospheric moisture, rainfall, and net absorbed clear-sky SW radiation (Figure 1). SST and LT have the largest negative values of  $r_i\{S, X\}$ . Rainfall has the weakest correlations with SAOD, due to a real difference in signal strength and/or

because rainfall is inherently noisy in space and time [Santer *et al.*, 1994], hampering reliable estimation of the true volcanic drying signal.

Four of the climate variables examined here (TMT, TLT, PR, and SST) have records that start at least 5 years prior to Pinatubo. This allows sampling of Pinatubo-induced SAOD and climate signals at the end of 60 month windows with start dates in mid-1986 (see Figures 2a and 2b). In these four longer climate data sets,  $p$  values decrease from nonsignificant values to nearly zero as the end of the sliding 60 month window shifts from September 1991 to October 1991 (the time of the peak post-Pinatubo monthly mean SAOD in the Vernier *et al.* data set). After this transition point,  $p$  values remain close to zero for periods ranging from 1–2 years (PR) to roughly a decade (for near-global averages of SST, TMT, and TLT; see Figures 2c and 2d).

The shorter SSM/I precipitable water record starts in 1988 and does not permit sampling of Pinatubo-caused signals at the end of the 60 month sliding windows. For PW, therefore, the first 60 month analysis window already captures Pinatubo's effects on SAOD and atmospheric moisture, yielding  $p$  values less than 0.02 for the  $r_i\{S, X\}$  statistic. Anticorrelations between SAOD and PW remain significant for 6–7 years in the tropics and for a decade in near-global averages (Figures 2c and 2d and supporting information Figures S2a and S2b).

Because the CERES EBAF net clear-sky SW record begins in the early 21st century, it cannot be used to evaluate the effect of Pinatubo on SW. This analysis is possible with the longer ISCCP SW record. As in the case of the temperature and moisture variables, large anticorrelations between the Pinatubo-induced changes in SAOD and SW have  $p$  values that remain close to zero for approximately a decade after the initial sampling of Pinatubo effects (see supporting information Figures S3 and S4).

Consider next the impact of the Tavorvur and Nabro eruptions. We obtain large negative values of  $r_i\{S, X\}$  during 60 month periods which sample the effects of these volcanic events (Figures 2a and 2b). In tropical averages of the Vernier *et al.* SAOD data, the peak values for Tavorvur and Nabro are in November 2006 and September 2011, respectively. In the near-global SAOD averages, the corresponding peak values are slightly time shifted and occur in December 2006 and August 2011. The 60 month analysis period which starts in November 2006 and ends in October 2011 captures both the Tavorvur and Nabro SAOD maxima, as well as the initial climate effects of these eruptions. The timing of SAOD peaks relative to the moving 60 month window explains why  $r_i\{S, X\}$  becomes more negative (and  $p$  values decrease markedly) as the window start date shifts from October to November 2006 (Figures 2c and 2d). Many other sudden jumps in  $r_i\{S, X\}$  are similarly influenced by volcanic end-point effects.

For tropically averaged SST, TMT, and TLT data, values of  $r_i\{S, X\}$  are significant at the 5% level or better for all 60 month periods with start dates between November 2006 and November 2007 (Figure 2c and supporting information Figure S2c). Some of the tropical PW and SW results during this interval also achieve significance at the 5% level or better, but significance is not as long-lasting as in the case of the temperature variables. For tropical rainfall, no 60 month analysis period with a start date in the 21st century yields  $r_i\{S, X\}$  results significant at the 10% level.

Results for near-global averages are qualitatively and quantitatively different (Figure 2d and supporting information Figure S2d). All six climate variables have significant values of  $r_i\{S, X\}$  for at least some of the 60 month windows which sample the effects of Tavorvur and Nabro. While an early 21st century volcanic signal was not identifiable in tropical PR records, values of  $r_i\{S, X\}$  computed with near-global PR averages are statistically significant at the 10% level or better for two different 21st century analysis periods. The first period lasts nearly 3 years; it begins with 60 month windows which start in April 2002 and which sample Tavorvur's drying signal at the end of the window. The second period with significant  $r_i\{S, X\}$  values for near-global PR is for all 60 month windows with start dates after January 2008. This period captures large-scale PR signals caused by Sarychev, Merapi, and Nabro (Figure 1m).

The statistical significance of volcanically induced SST, PW, and SW signals is generally higher for near-global than for tropical averages (see Figures 2c, 2d, and 3). This result is partly due to the fact that near-global averages have smaller residual noise after statistical removal of ENSO effects (Figure 1). The higher significance levels of the near-global results may also be related to better spatial sampling of the climate signals of high-latitude eruptions (such as Kasatochi in 2008 and Sarychev in 2009).

Figure 3 summarizes the overall significance of the individual 60 month tests. The Figure shows PCNT, the percentage of significant  $r_i\{S, X\}$  values. Results are a function of climate variable and averaging domain. Because of the combined effects of temporal autocorrelation and relatively short observational records,

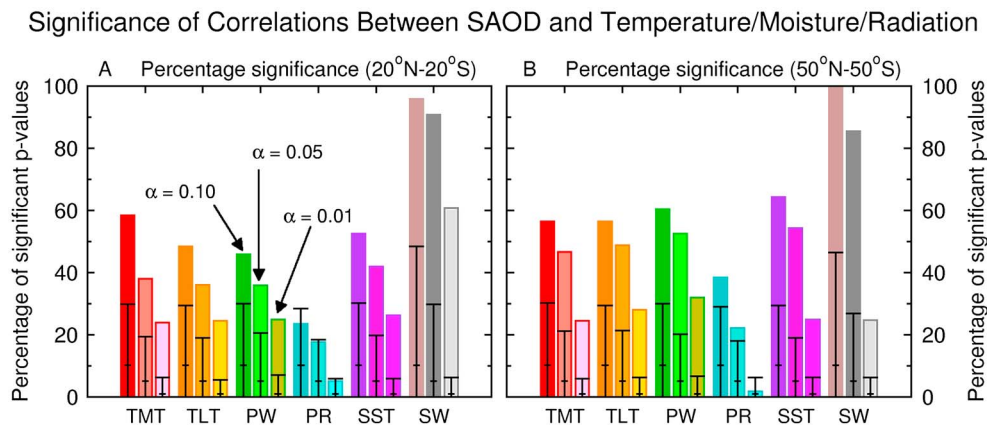


**Figure 3.** Observed values of PCNT, the percentage of the total number of individual “sliding window” tests of  $r_i\{S, X\}$  yielding results that are statistically significant at three stipulated significance levels (10%, 5%, and 1%; these are the left, middle, and right bars for each variable). Results are for temporal correlations between SAOD and climate data spatially averaged (a) over the tropics and (b) over a near-global domain. The figure synthesizes the  $p$  value information presented in Figures 2c and 2d. The black bars were obtained from the Monte Carlo-generated null distributions of PCNT\* and provide information on the significance of observed PCNT results. The length of each black bar spans the 5% to 95% confidence range of the 1000-member null distribution of PCNT\* results; the horizontal line is plotted at the average of the null distribution. Further significance testing details are given in the SI.

it is difficult to estimate the number of independent samples of  $r_i\{S, X\}$ . For each climate variable, therefore, it is difficult to determine whether the observed PCNT value is statistically unusual. Nonindependence of the individual tests of  $r_i\{S, X\}$  is due to two factors: (1) temporal autocorrelation in the observed climate and SAOD data and (2) our use of maximally overlapping 60 month windows to account for nonstationarity of volcanic activity.

Here we employed a Monte Carlo approach to generate null distributions of PCNT\* with synthetic SAOD time series and observational climate data. This approach allows us to determine whether each observed PCNT value in Figure 3 reflects true volcanically induced climate signals or could instead be due to the combined effects of nonindependent tests and purely random correspondence between fluctuations in SAOD and in climate (see Figures S5 and S6 and section 3 of the supporting information). Our analysis suggests that in almost all cases examined here, observed PCNT values are too large to be explained by a combination of chance and nonindependent tests. For tests involving tropical average PR data, however, observed values of PCNT cannot be confidently discriminated from the Monte Carlo-derived null distributions of PCNT\*.

One feature of interest in Figures 2 and 3 relates to the SW results. In contrast to temperature and moisture, the SW response to volcanically induced SAOD changes is highly significant over most of the 21st century and displays noticeably different temporal variability of  $r_i\{S, X\}$ . This is probably due to several effects. First, net clear-sky SW radiation at the top of the atmosphere responds more directly to SAOD changes and is less affected by internal variability than the tropospheric temperature and moisture variables considered here. Second, volcanically induced signals in SAOD and net clear-sky SW radiation have relatively short decay times. Decay times are longer for tropospheric temperature and moisture signals, which are attenuated by the thermal inertia of the oceanic mixed layer. SW anomalies are therefore more synchronous with volcanically driven changes in SAOD. All of these factors contribute to the very large observed PCNT values for tests involving SW data (Figure 3).

### 7. Explained Variance Results

In this section, we provide information on volcanic signal strength in observational climate data. We first determine  $V_{RES}$ , the residual temporal variance after ENSO removal from tropical and near-global averages of TMT, TLT, PR, PW, and SST. We then use  $V_{RES}$  and values of  $r_i\{S, X\}^2$  from Figures 2a and 2b to calculate  $V_{RAW}$ , the percentage of the temporal variance of the original temperature and moisture data that is due to fluctuations in the Vernier et al. SAOD. As in Figure 2, this calculation is performed with maximally overlapping 60 month windows to address nonstationarity in volcanic activity. Since it was not necessary

Temporal Variance Explained by Stratospheric Aerosol Optical Depth

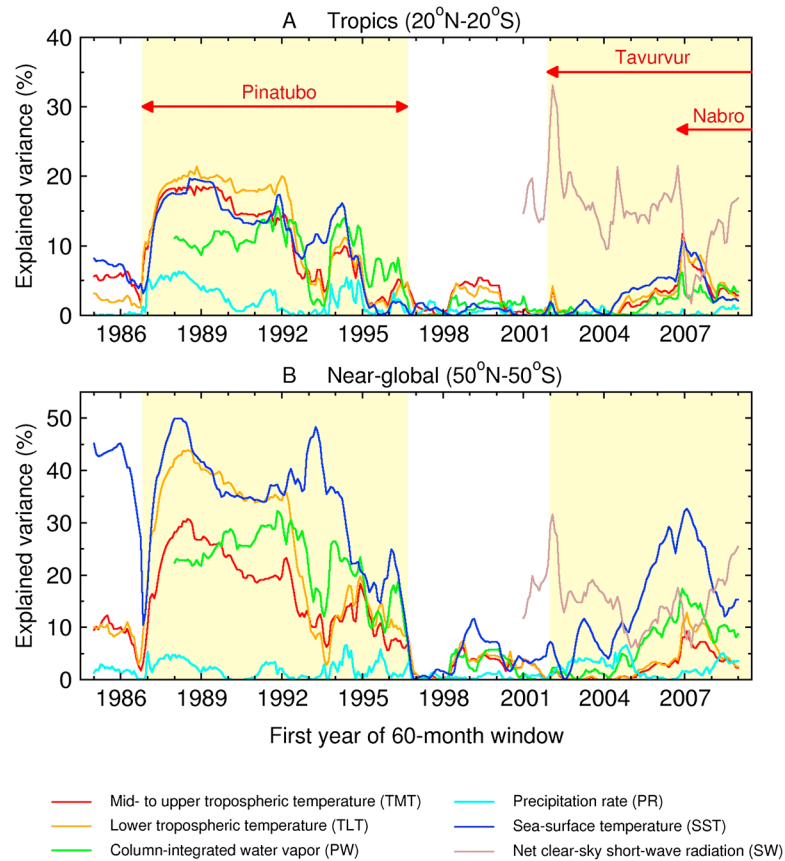


**Figure 4.**  $V_{RAW}$ , the percentage of the temporal variance of the original temperature, moisture, and radiation data explained by changes in SAOD. Results are for climate and SAOD data spatially averaged (a) over the tropics (20°N–20°S) and (b) over a near-global domain (50°N–50°S).  $V_{RAW}$  is simply  $[V_{RES} \times r_i \{S, X\}^2] \times 100$ , where  $V_{RES} = (1 - r\{ENSO, X\}^2)$ , and  $r\{ENSO, X\}^2$  is the variance explained by ENSO after application of the iterative method for statistical separation of the climate signals arising from ENSO and Pinatubo. For an explanation of the yellow boxes, refer to the caption of Figure 2.

to remove ENSO effects from SW data, the explained variance calculation for SW does not require use of residual variance information.

The temperature and moisture variance explained by SAOD is systematically larger in near-global averages than in tropical averages (Figure 4). For example, in the case of SST variability during the Pinatubo period, SAOD explains between 35 and 50% of the variance of near-global averages but no more than 20% of the variance of tropical averages. This result is partly due to geographical differences in the size of the ENSO contribution to climate variability. For all temperature and moisture data analyzed here, ENSO explains considerably more of the temporal variance in tropical averages than in near-global averages (e.g.,  $r\{ENSO, SST\}^2 = 0.674$  for tropical SST and 0.225 for near-global SST). Differences between the tropical and near-global  $V_{RAW}$  results in Figure 4 must also be related to the spatial sampling of low-latitude and high-latitude volcanic cooling signals (see above).

During the period influenced by the eruptions of Soufrière Hills, Tavorvur, and Nabro, the peak values of  $V_{RAW}$  exceed 30% for near-global averages of SST (Figure 4b). Clearly, the amplitude of these recent volcanic cooling signals is not negligible. The largest post-Pinatubo cooling signals are preferentially distributed in the final third of the “warming hiatus” period and must therefore contribute to the hiatus.

### 8. Sensitivity Tests

We performed a number of sensitivity tests to investigate the impact of different processing choices on our results (see supporting information and Figures S7–S10). These tests involved the following: (1) varying the



window length in the correlation calculations; (2) assessing the significance of the regression coefficients between  $S(t)$  and  $X(t)$ ; (3) varying the temporal lags between SAOD and the temperature and moisture variables; (4) considering the impact of uncertainties in  $a_1$ , the lag-1 autocorrelation in the AR-1 model used for generating synthetic climate data; and (5) retaining ENSO variability. We focus on test (5) here and note that tests (1) through (4) do not result in conclusions that are fundamentally different from those derived using the default choices in the paper.

If ENSO effects are retained, significance results are radically different: a Pinatubo signal is only identifiable for near-global TLT data, and 60 month periods sampling both Tavurvur and Nabro yield only marginally significant  $r_i\{S, X\}$  values (cf. Figures 2 and S10). These null results are due to two effects: the masking of underlying volcanic climate signals by ENSO variability and the higher temporal autocorrelation in the synthetic climate time series. ENSO removal is therefore essential to the successful identification of the climate signals induced by Pinatubo and some of the larger early 21st century volcanic eruptions.

## 9. Discussion

Our volcanic signal detection results for tropical and near-global temperature, moisture, and SW radiation are directly relevant to a recent claim that “the current hiatus is part of natural climate variability, tied specifically to a La Niña-like decadal cooling” [Kosaka and Xie, 2013]. This conclusion was based on a climate model simulation in which observed time-varying SST changes were specified over a domain encompassing the eastern equatorial Pacific—a region strongly influenced by ENSO variability. The simulation replicated many key aspects of the observed post-1998 “warming hiatus,” thus providing some justification for the claim mentioned above.

Our findings show that the hiatus is not due to internal variability alone. We have identified statistically significant, externally forced volcanic signals in multiple, independently monitored climate variables. Of particular interest is our positive detection of volcanic cooling signals in observed tropical SST data. These signals are discernible for the 1991 Pinatubo eruption and for several of the larger early 21st century eruptions. Volcanic cooling signals are therefore aliased into the observed tropical SST changes specified by Kosaka and Xie [2013]. Other external forcings could also affect these SSTs [Meehl et al., 2009]. While prescribed SST simulations are useful for many purposes [see, e.g., Gates et al., 1999], our study shows that they cannot reliably quantify the contributions of individual factors to the “warming hiatus.”

In summary, we have demonstrated that tropical and near-global signals of late 20th and early 21st century volcanic activity exist in a variety of different observational climate records. These cooling, drying, and backscattering signals are internally consistent and are interpretable in terms of basic physical mechanisms [Robock, 2000; Soden et al., 2002; Gillett et al., 2004; Ramaswamy et al., 2006; Solomon et al., 2011; Fyfe et al., 2013a]. While there is still considerable quantitative uncertainty in the volcanic contribution to the “warming hiatus,” this uncertainty is likely to decrease with improved observational understanding of volcanically induced SAOD changes and with improved representation of volcanic forcing in model simulations.

## References

- Adler, R. F., et al. (2003), The version 2.1 Global Precipitation Climatology Project (GPCP) monthly precipitation analysis (1979–present), *J. Hydrometeorol.*, *4*, 1147–1167.
- Broccoli, A. J., K. W. Dixon, T. L. Delworth, T. R. Knutson, R. J. Stouffer, and F. Zeng (2003), Twentieth century temperature and precipitation trends in ensemble climate simulations including natural and anthropogenic forcing, *J. Geophys. Res.*, *108*(D24), 4798, doi:10.1029/2003JD003812.
- Chen, X., and K. K. Tung (2014), Varying planetary heat sink led to global-warming slowdown and acceleration, *Science*, *345*, 897–903.
- Flato, G., et al. (2013), Evaluation of climate models, in *Climate Change 2013: The Physical Science Basis. Contribution of Working Group I to the Fifth Assessment Report of the Intergovernmental Panel on Climate Change*, edited by T. F. Stocker et al., Cambridge Univ. Press, Cambridge, U. K., and New York.
- Fyfe, J. C., K. von Salzen, J. N. S. Cole, N. P. Gillett, and J.-P. Vernier (2013a), Surface response to stratospheric aerosol changes in a coupled atmosphere-ocean model, *Geophys. Res. Lett.*, *40*, 584–588, doi:10.1002/grl.50156.
- Fyfe, J. C., N. P. Gillett, and F. W. Zwiers (2013b), Overestimated global warming over the past 20 years, *Nat. Clim. Change*, *3*, 767–769.
- Gates, W. L., et al. (1999), An overview of the results of the Atmospheric Model Intercomparison Project (AMIP I), *Bull. Am. Meteorol. Soc.*, *80*, 29–55.
- Gillett, N. P., A. J. Weaver, F. W. Zwiers, and M. F. Wehner (2004), Detection of volcanic influence on global precipitation, *Geophys. Res. Lett.*, *31*, L12217, doi:10.1029/2004GL020044.
- Harries, J. E., and J. M. Fuyuan (2006), On the stability of the Earth's radiative energy balance: Response to the Mt. Pinatubo eruption, *Geophys. Res. Lett.*, *33*, L23814, doi:10.1029/2006GL027457.

### Acknowledgments

All observational climate data used here are in the public domain, available at the following locations: (1) <http://www.remss.com/data> (for TMT, TLT, and PW); (2) <http://www.ncdc.noaa.gov/oa/climate/research/sst> (for SST); (3) <http://ceres-tool.larc.nasa.gov/ord-tool/> (for SW); and (4) <http://www.esrl.noaa.gov/psd/data/gridded/data.gpcp.html> (for PR). We thank Tom Wigley (University of Adelaide) for valuable comments and suggestions. At Lawrence Livermore National Laboratory, work by B.D.S., J.P., and M.Z. was performed under the auspices of the US Department of Energy under contract DE-AC52-07NA27344; C.B. was supported by the DOE/OBER Early Career Research Program Award SCW1295. S.S. was supported in part by NSF grant AGS-1342810.

The Editor thanks two anonymous reviewers for their assistance in evaluating this paper.

- Huber, M., and R. Knutti (2014), Natural variability, radiative forcing and climate response in the recent hiatus reconciled, *Nat. Geosci.*, *7*, 651–656, doi:10.1038/NGEO2228.
- Iles, C. E., and G. C. Hegerl (2014), The global precipitation response to volcanic eruptions in the CMIP5 models, *Environ. Res. Lett.*, *9*, 104012, doi:10.1088/1748-9326/9/10/104012.
- Kaufmann, R. K., H. Kauppi, M. L. Mann, and J. H. Stock (2011), Reconciling anthropogenic climate change with observed temperature 1998–2008, *Proc. Natl. Acad. Sci. U.S.A.*, *108*, 11,790–11,793.
- Kopp, G., and J. L. Lean (2011), A new, lower value of total solar irradiance: Evidence and climate significance, *Geophys. Res. Lett.*, *38*, L01706, doi:10.1029/2010GL045777.
- Kosaka, K., and S.-P. Xie (2013), Recent global-warming hiatus tied to equatorial Pacific surface cooling, *Nature*, *501*, 403–407, doi:10.1038/nature12534.
- Loeb, N. G., B. Wielicki, D. R. Doelling, G. L. S. Smith, D. F. Keyes, S. Kato, N. Manalo-Smith, and T. Wong (2009), Toward optimal closure of the Earth's top-of-atmosphere radiation budget, *J. Clim.*, *22*, 748–766.
- Mears, C. A., B. D. Santer, F. J. Wentz, K. E. Taylor, and M. F. Wehner (2007), Relationship between temperature and precipitable water changes over tropical oceans, *Geophys. Res. Lett.*, *34*, L24709, doi:10.1029/2007GL031936.
- Mears, C., F. J. Wentz, P. Thorne, and D. Bernie (2011), Assessing uncertainty in estimates of atmospheric temperature changes from MSU and AMSU using a Monte-Carlo technique, *J. Geophys. Res.*, *116*, D08112, doi:10.1029/2010JD014954.
- Meehl, G. A., J. M. Arblaster, K. Matthes, F. Sassi, and H. van Loon (2009), Amplifying the Pacific climate system response to a small 11-year solar cycle forcing, *Science*, *325*, 1114–1118.
- Neely, R. R., III et al. (2013), Recent anthropogenic increases in SO<sub>2</sub> from Asia have minimal impact on stratospheric aerosol, *Geophys. Res. Lett.*, *40*, 999–1004, doi:10.1002/grl.50263.
- Ramaswamy, V., M. D. Schwarzkopf, W. J. Randel, B. D. Santer, B. J. Soden, and G. L. Stenchikov (2006), Anthropogenic and natural influences in the evolution of lower stratospheric cooling, *Science*, *311*, 1138–1141.
- Ridley, D. A., et al. (2014), Total volcanic stratospheric aerosol optical depths and implications for global climate change, *Geophys. Res. Lett.*, *41*, 7763–7769, doi:10.1002/2014GL061541.
- Robock, A. (2000), Volcanic eruptions and climate, *Rev. Geophys.*, *38*, 191–219.
- Santer, B. D., W. Brüggemann, U. Cubasch, K. Hasselmann, E. Maier-Reimer, and U. Mikolajewicz (1994), Signal-to-noise analysis of time-dependent greenhouse warming experiments, *Clim. Dyn.*, *9*, 267–285.
- Santer, B. D., T. M. L. Wigley, C. Doutriaux, J. S. Boyle, J. E. Hansen, P. D. Jones, G. A. Meehl, E. Roeckner, S. Sengupta, and K. E. Taylor (2001), Accounting for the effects of volcanoes and ENSO in comparisons of modeled and observed temperature trends, *J. Geophys. Res.*, *106*, 28,033–28,059.
- Santer, B. D., et al. (2014), Volcanic contribution to decadal changes in tropospheric temperature, *Nat. Geosci.*, *7*, 185–189.
- Schmidt, G. A., D. T. Shindell, and K. Tsigaridis (2014), Reconciling warming trends, *Nat. Geosci.*, *7*, 158–160.
- Smith, T. M., R. W. Reynolds, T. C. Peterson, and J. Lawrimore (2008), Improvements to NOAA's historical merged land-ocean surface temperature analysis (1880–2006), *J. Clim.*, *21*, 2283–2296.
- Soden, B. J., R. T. Wetherald, G. L. Stenchikov, and A. Robock (2002), Global cooling after the eruption of Mount Pinatubo: A test of climate feedback by water vapor, *Science*, *296*, 727–730.
- Solomon, S., K. H. Rosenlof, R. W. Portman, J. S. Daniel, S. M. Davis, T. J. Sanford, and G. K. Plattner (2010), Contributions of stratospheric water vapor to decadal changes in the rate of global warming, *Science*, *327*, 1219–1223.
- Solomon, S., J. S. Daniel, R. R. Neely, J.-P. Vernier, E. G. Dutton, and L. W. Thomason (2011), The persistently variable “background” stratospheric aerosol layer and global climate change, *Science*, *333*, 866–870.
- Thompson, D. W. J., J. M. Wallace, P. D. Jones, and J. J. Kennedy (2009), Identifying signatures of natural climate variability in time series of global-mean surface temperature: Methodology and insights, *J. Clim.*, *22*, 6120–6141.
- Trenberth, K. E., J. T. Fasullo, G. Branstator, and A. S. Phillips (2014), Seasonal aspects of the recent pause in surface warming, *Nat. Clim. Change*, *4*, 911–916, doi:10.1038/NCLIMATE2341.
- Vernier, J.-P., et al. (2011), Major influence of tropical volcanic eruptions on the stratospheric aerosol layer during the last decade, *Geophys. Res. Lett.*, *38*, L12807, doi:10.1029/2011GL047563.
- Wigley, T. M. L. (2000), ENSO, volcanoes, and record-breaking temperatures, *Geophys. Res. Lett.*, *27*, 4101–4104.
- Wigley, T. M. L., C. M. Ammann, B. D. Santer, and S. C. B. Raper (2005), The effect of climate sensitivity on the response to volcanic forcing, *J. Geophys. Res.*, *110*, D09107, doi:10.1029/2004/JD005557.
- Zhang, Y., W. B. Rossow, A. A. Lacis, V. Oinas, and M. I. Mishchenko (2004), Calculation of radiative fluxes from the surface to top of atmosphere based on ISCCP and other global data sets: Refinements of the radiative transfer model and the input data, *J. Geophys. Res.*, *109*, D19105, doi:10.1029/2003JD004457.